International Journal of Civil Engineering
https://doi.org/10.1007/s40999-018-0337-5

RESEARCH PAPER

Influence of Abutment Slope Angle Variety on the Deformation and Stress of the Concrete-Faced Rockfill Dam During Initial Impoundment

Ruihu Song[1] · Junrui Chai[1,2] · Zengguang Xu[1] · Yuan Qin[1] · Jing Cao[1,3]

Received: 24 October 2017 / Revised: 21 May 2018 / Accepted: 3 June 2018

Abstract
Favorable valley terrain for building dams is gradually decreasing. The primary objective of this study is to investigate the influence of abutment slope angle variety on the deformation and stress of concrete-faced rockfill dam (CFRD). First, the effect of abutment slope angle on perimeter joint deformation is investigated using CFRD monitoring data in China. A normalized deformation index (C_{DS}) is proposed to evaluate the relationship between perimeter joint deformation and the steepest abutment slope angle. Results indicate that perimeter joint deformation increases nonlinearly with the steepest abutment slope angle. Then, numerical analysis is conducted on Miaojiaba CFRD under three types of abutment slope variety from upstream to downstream. We focus on the effect of abutment slope angle variety from upstream to downstream on CFRD behavior. In the analysis, the terrain shape line is assumed to be constant at the downstream slope foot, and the abutment slope angle increases linearly from upstream to downstream. The Duncan–Chang E–B model is used in nonlinear analysis for rockfill, and the slab–rockfill interfaces are modeled using contact elements with Coulomb friction. An influence sphere is proposed for the different types of abutment slope angles. Results indicate that face slab deformation is more dependent on abutment slope angle than rockfill deformation.

Keywords Valley terrain · Abutment slope angle · Concrete-faced rockfill dam · Deformation · Stress

1 Introduction

With the development of water resources and hydropower engineering, concrete-faced rockfill dams (CFRDs) are increasingly being adopted in many cases given their advantages of simple detailing, short construction periods, and inherent resistance to earthquake loading. In the past two decades, many high or ultrahigh CFRDs have been built throughout the world using innovative filling methods and new materials. Meanwhile, many CFRDs that are more than 100 m in height are either completed, under construction, or planned [1]. Favorable valley terrain for building dams is gradually decreasing. As a result, many CFRDs will have to be built on complex valley terrain and alluvium. Thus, the safety of CFRDs in these areas has become increasingly important.

Numerous factors influence the stress–deformation properties of CFRDs. In general, two sorts of factors are involved: internal and external factors. Internal factors refer to the properties of the CFRDs itself, such as dam height, rockfill properties, and quality of rockfill compaction.

✉ Junrui Chai
jrchai@xaut.edu.cn

Ruihu Song
ruihu_xaut@163.com

Zengguang Xu
xuzengguang@xaut.edu.cn

Yuan Qin
lanelyly@163.com

Jing Cao
caojingxn@163.com

[1] State Key Laboratory of Eco-hydraulics in Northwest Arid Region of China, Xi'an University of Technology, Xi'an 710048, People's Republic of China

[2] School of Civil Engineering, Xijing University, Xi'an 710123, People's Republic of China

[3] State Key Laboratory of Geo-Information Engineering, Xi'an 710054, People's Republic of China

Published online: 11 June 2018

External factors refer to the objective factors that are not determined by the designer in advance, such as the groundwater level, valley terrain, and depth of the alluvium.

At present, some investigators have focused their work on the influences of dam height and rockfill properties on the stress and deformation of CFRDs. Hunter and Fell [2] presented a method for estimating the modulus of compacted rockfill in dams on the bases of particle size, unconfined compressive strength of the rock, compaction layer thickness, compactive effort, and applied vertical stress. Panos Dakoulas [3, 4] conducted a comprehensive study on the nonlinear seismic response of high CFRDs in narrow canyons and provided insight into the effect of longitudinal vibrations on the seismic behavior of CFRDs. Mu-Kwang Kim et al. [5] investigated the seismic behavior of earth-core rockfill dams (ECRDs) and CFRDs with dynamic centrifuge tests. Bin Xu and Degao Zou [6] established a modified generalized plasticity model for rockfill materials. This model has been applied to Zipingpu CFRD in China to evaluate its rationality. Other investigators proposed several algorithms to analyze and predict the deformation of CFRDs. Mehdi Modares et al. [7] developed a new framework that can predict the possible failure of a face slab in CFRD and used a case study to validate the results. Yong-Seong Kim and Byung-Tak Kim [8] developed a neural network model to predict the relative crest settlement of CFRD, and their results are consistent with field data. Wei Zhou and Junjie Hua [9] applied hybrid genetic algorithms to the back-analysis of the Shuibuya CFRD and verified the back-analysis method with in situ settlement records.

As mentioned before, complex valley terrain and alluvium have become new challenges for CFRD construction. A number of studies have investigated the physical, mechanical, and hydraulic properties of alluvium [10–12] and the behavior of dams founded on such alluvium [13–20]. The effect of valley terrain on face slab and stresses within the dam has been investigated in some published works [2, 7]. However, they considered only one factor and did not conduct comprehensive studies on the effects of alluvium and valley terrain on CFRDs. CFRDs present new deformation features under the common effect of alluvium and valley terrain. Thus, a comprehensively analyze the influence of a complex valley terrain on the deformation of CFRDs built on alluvium is necessary.

In this study, the effect of abutment slope angle on perimeter joint deformation is investigated using CFRD monitoring data in China. A normalized deformation index (C_{DS}) is proposed to evaluate the relationship between perimeter joints deformation and the steepest abutment slope angle.

Finite element (FE) analysis is conducted to simulate the construction and initial impoundment process of the Miaojiaba CFRD, which was built on a river gravel foundation in China. We focus on the effect of abutment slope angle variety from upstream to downstream on CFRD behavior. In the analysis, the terrain shape line is assumed to be constant at the downstream slope foot, and abutment slope angle increases linearly from upstream to downstream. The Zipingpu CFRD is presented as a case study to illustrate the generality of our results. The results of this study offer useful insight into the effect of abutment slope angle on the behavior of CFRD built on alluvium.

2 Literature Review: Influence of Abutment Slope Angle on the Deformation of CFRDs

Many factors [21] affect the deformation of CFRDs, including dam height, rockfill properties, particle gradation, rolling parameters, construction quality, valley terrain, and alluvium depth. However, the observed behavior of CFRDs during reservoir impounding has shown that the effect of valley terrain on the safety of the impermeable barrier is significant. Table 1 shows the perimeter joint deformation and characteristic parameters of high CFRDs in China. In the table, the effect of dam height (H) and vertical compression modulus (E_v) is considered in the computation of characteristic value of the perimeter joint deformation (C_{DS}). C_{DS} is a normalized deformation index of the perimeter joint deformation. D_S and C_{DS} can be expressed as follows:

$$D_s = \sqrt{O^2 + S^2 + T^2} \tag{1}$$

$$C_{DS} = {}^{D_s * E_v}/_{H} \tag{2}$$

where O is the tensile deformation along the dam axis, S is the settlement deformation perpendicular to the face slab, and T is the shear deformation along the dam slope.

E_v [22] can be expressed as

$$E_v = \frac{\gamma DH}{s} \tag{3}$$

where γ is the unit weight of the rockfill, D is the depth of the rockfill above the settlement gauge, H is the height of the rockfill below the settlement gauge, and s is the settlement of the gauge (Fig. 1).

Details of the valley terrain and parameters of dams are collected. The observed behavior of high CFRDs has been studied based on completed cases. The influence of valley terrain on the impermeable barrier is summarized as follows:

1. The distribution of the characteristic value of the perimeter joint deformation versus the steepest abutment slope angle is shown in Fig. 2. The perimeter joint deformation increases nonlinearly with the steepest abutment slope angle possibly because the rockfill slides under oversteepened slope and subsequently drags face slab

Table 1 Perimeter joint deformation and characteristic parameters of high CFRDs in China

Dam	Completion year	Height (H/m)	Thickness of alluvium (m)	Rockfill material	Valley terrain	Perimeter joint deformation (mm)			α_{max}/°	E_v/MPa	D_s/mm	C_{DS}/kPa
						O	S	T				
Tianshengqiao-1	1998	178.0	0	Limestone, sand shale	Wide V-shaped Left abutment slope 20°–30° Right abutment slope 18°–30°	20.9	28.5	20.8	30	50.9	41.0	11.7
Sanbanxi	2007	185.5	0	Siltstone, tuffaceous sandstone plywood	Slightly asymmetric V-shaped Left abutment slope 40°–52° Right abutment slope 45°–60°	71.8	50.2	58.6	60	96.7	105.4	54.9
Hongjiadu	2005	179.5	0	Limestone shaly sandstone	Asymmetric V-shaped Left abutment slope average 70° Right abutment slope 25°–40°	13.9	26.6	34.8	70	135.2	46.0	34.6
Jilintai-1	2006	157.0	0	Sand gravel, tuff	Symmetric V-shaped Left abutment slope average 35°–70° Right abutment slope 25°–40°	11.9	35.1	3.5	45	132.7	37.1	31.4
Dongjing	2009	149.5	0	Sand shale	Slightly asymmetric V-shaped Left abutment slope average 35° Right abutment slope 25°–28°	18.4	34.3	20.8	35	57.9	44.1	17.1
Longshou-2	2004	146.5	0	Bright green porphyry	Slightly asymmetric V-shaped Left abutment slope average 70° Right abutment slope steep alternately	15.0	15.5	16.5	70	–	21.6	–
Gongboxia	2005	132.2	0	Granite, schist	Asymmetric V-shaped Left abutment slope average 30° Right abutment slope 40°–50°	26.1	45.4	21.4	50	133.1	56.6	57.0
Yinzidu	2004	129.5	0	Limestone, mudstone	Slightly asymmetric U-shaped Left abutment slope average 70°–80° Right abutment slope 45°	24.7	26.0	30.7	70	53.5	47.2	19.5
Jiudianxia	2008	136.0	56.0	Limestone	Asymmetric V-shaped Left abutment slope average 80° Right abutment slope 40°–50°	61.0	43.0	25.0	80	129.4	78.7	74.9
Shuibuya	2008	233.0	14.0	Limestone	Asymmetric V-shaped Left abutment slope average 52° Right abutment slope average 35°	13.0	45.7	43.7	52	118.6	64.6	32.9
Tankeng	2009	162.0	23.5	Sand gravel volcanic mass rock	Symmetric V-shaped Left abutment slope 35°–50° Right abutment slope 45°–52°	13.8	39.8	11.8	50	132.7	48.3	39.6

Table 1 (continued)

Dam	Completion year	Height (H/m)	Thickness of alluvium (m)	Rockfill material	Valley terrain	Perimeter joint deformation (mm)			α_{max}/°	E_v/MPa	D_s/mm	C_{DS}/kPa
						O	S	T				
Zipingpu	2006	158.0	11.0	Limestone sand gravel	Symmetric V-shaped	15.2	10.8	27.4	50	110.1	33.1	23.1
					Left abutment slope 40°–50°							
					Right abutment slope 20°–25°							
Shanxi	2001	132.5	20.2	Rhyolite sand gravel	Slightly asymmetric U-shaped	6.2	15.0	8.1	45	85.9	18.1	11.7
					Left abutment slope 30°–40°							
					Right abutment slope 40°–45°							
Miaojiaba	2011	111.0	44.0	Tuff	Symmetric V-shaped	19.0	18.9	11.8	45	47.1	29.3	13.1
					Left abutment slope 42°–45°							
					Right abutment slope 42°–45°							

O tensile deformation along the dam axis, *S* settlement deformation perpendicular to the face slab, *T* shear deformation along the dam slope, α_{max} steepest abutment slope angle, E_v vertical modulus of deformation, D_s total deformation of the perimeter joint, C_{DS} perimeter joint deformation characteristic value that is considered the effects of dam height (H) and vertical compression modulus (E_v)

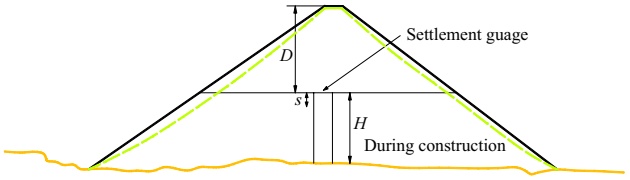

Fig. 1 Vertical settlements during construction

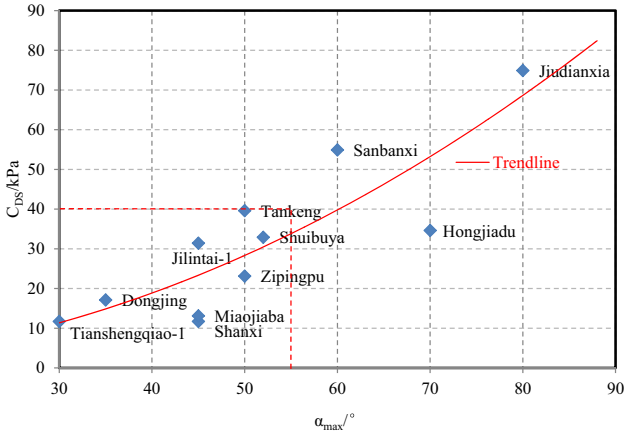

Fig. 2 Distribution of the characteristic value of the perimeter joints deformation versus the steepest abutment slope angle

movement. The steepest abutment slope angle of most cases is less than 55°. The characteristic value will increase slightly with the steepest abutment slope angle under the condition that it is less than 55°. Thus, the recommended steepest abutment slope angle is less than 55°. However, Hongjiadu is an outlier mainly because a special compaction zone is adopted in the oversteepened slope.

2. The excavation shape of the abutment slope at the dam site, particularly the upstream of the dam axis, significantly affects the cushion zone deformation and concrete face slab deformation. The concrete slab cracking observed on the Xingó and Itapebi CFRDs [23] presents slab sliding and considerable concrete spalling. The cause of slab cracking in the Xingó CFRD is the sharp geometry of the left abutment and Zone 3C material deformability. The cause of cracks parallel to the plinth in the Itapebi CFRD is foundation geometry.
3. The width of the valley affects the deformation of concrete slabs. Wide valleys have few constraints on the rockfill and concrete slabs, such that concrete slabs deflection are prominent in wide valleys, thereby causing the perimeter and vertical joints to have large tensile deformation. By contrast, narrow valleys have an arching effect, which limits the rockfill and concrete slab deformation. As a result, the concrete slab deflection and

perimeter joint tensile deformation are small. However, the shear deformation of the joints along the dam slope is prominent because the deformation of the dam caused by the load is mainly concentrated in the vertical settlement. These effects are prominent in the Golillas Dam [24] and the Anchicaya Dam.

4. The concrete slabs and perimeter joints are weak at the abutment slope bend, thereby causing perimeter joint spalling or perimeter joint cracking. Examples of this case are the perimeter joint fractures in the Xingo and Shuibuya dams.
5. An asymmetric valley terrain significantly affects the distribution of concrete slab deformation. The concrete slab deformation along the dam axis near the steep abutment slope is larger than that near the flat abutment slope. This feature is prominent in the Hongjiadu Dam. Reduction of concrete slab width at the steep abutment slope is an effective mitigation measure to minimize the potential for cracks on the concrete slabs.

The concrete slab cracking observed on several CFRDs presents compressive or tensile failures, including slab heaving, considerable concrete spalling, and slab sliding. These failures indicate that considering the valley terrain for constructing CFRD is important. Thus, dam designers should pay attention to valley terrain in all factors that most likely contribute to the observed behavior during reservoir impounding. We conduct numerical analysis on the Miaojiaba CFRD, which is built on alluvium in China, to comprehensively investigate the behavior of CFRD built on alluvium. The description of the Miaojiaba CFRD and the numerical analysis are discussed in the following section.

3 Miaojiaba CFRD

3.1 Characteristics of the Miaojiaba CFRD

The Miaojiaba CFRD is located in the downstream of the Bailongjiang River, Wenxian, Gansu Province, China. The dam was designed with a maximum height of 111 m and a crest length of 348.2 m. It has a storage capacity of 2.68 billion m^3. The powerhouse has an installed capacity of 240 MW. The annual energy generation is 9.24×10^9 kWh. The valley terrain and layout view of the Miaojiaba CFRD is shown in Fig. 3. The material zoning is presented on a cross section in Fig. 4. Table 2 shows the material zone properties of the Miaojiaba CFRD. A 5.2 m high L-shaped concrete parapet wall at the upstream of the crest connects with the slab in the upstream. The upstream slope is 1v:1.4 h, and the downstream local slopes are 1v:1.35 h and 1v:1.4 h.

3.2 Geology and Valley Terrain at the Dam Site

The dam is located in an alpine valley. As shown in Fig. 4, the site has 44–48 m deep alluvium. The alluvium from

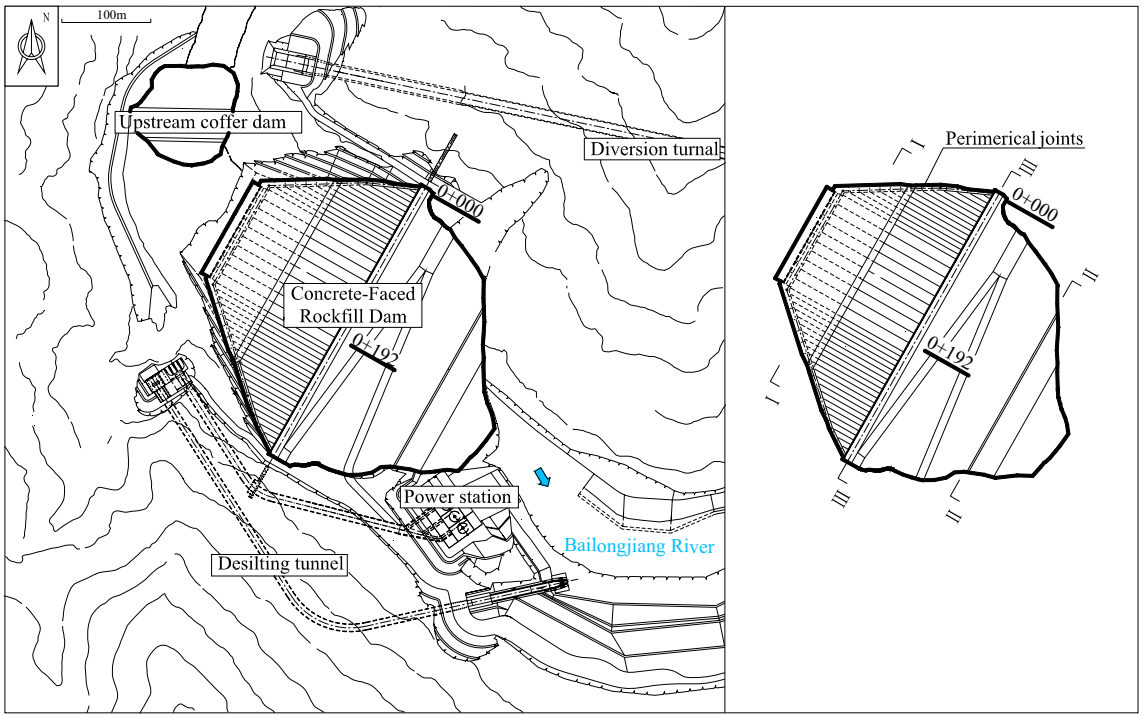

Fig. 3 Valley terrain and layout of the Miaojiaba CFRD

the bottom to the top can be divided as follows: $Q_4^{al}-1$ (sand and gravel with block gravel layers; 5 m to 10 m thick), $Q_4^{al}-2$ (sand and gravel; 12–15 m thick), $Q_4^{al}-3$ (cobble, sand, and gravel with gravel layers; 6–20 m thick), and $Q_4^{al}-4$ (reservoir alluvium; 2–4 m thick). The $Q_4^{al}-4$ alluvium is excavated during the construction of the CFRD. As shown in Fig. 3, the dam site is located at the river bend, and the valley terrain varies significantly at the dam site. Cross-sections I–I and II–II of the valley terrain are shown in Fig. 5. The left abutment slope gradually becomes flat from upstream to downstream and the river is deflected toward the right bank from upstream to downstream at the dam site.

4 Numerical Analysis

4.1 Constitutive Model

The behavior of CFRDs has been studied by a number of investigators using nonlinear analysis. They proposed a series of constitutive models to simulate the behavior of rockfill. Various models are applied to investigate CFRD deformation behavior in different periods. The

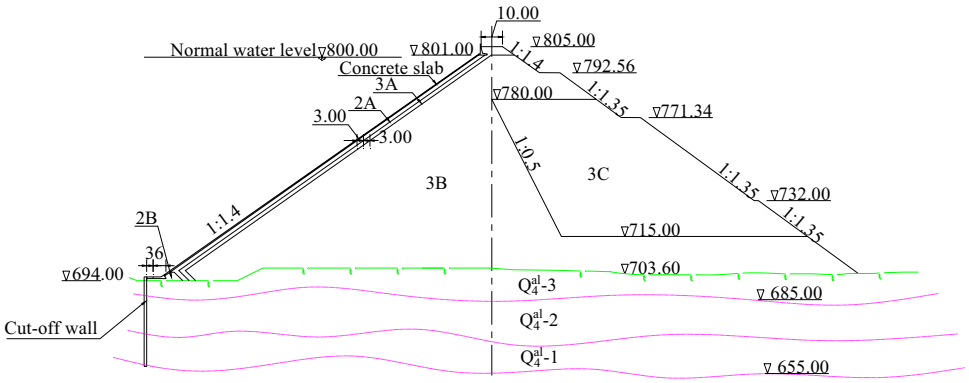

Fig. 4 Material zoning of the Miaojiaba CFRD

Table 2 Material zone properties of the Miaojiaba CFRD

Zone	Properties
Concrete slab	Variable thickness is reduced with height based on the formula $0.3+0.003H$
ZONE 2A	Cushion zone is composed of blended sand and gravel, with a maximum particle size of 150 mm. This zone is immediately behind the face slab
ZONE 2B	Special cushion zone
ZONE 3A	Transition zone is composed of selected rock and processed metamorphic tuff, with a maximum particle size of 300 mm. This zone is placed adjacent to Zone 2B
ZONE 3B	Main rockfill zone consists of quarry rock and metamorphic tuff
ZONE 3C	Sub-rockfill zone is located downstream and layer thickness is about 0.85 m. This zone has the same components as Zone 3B but has a different density

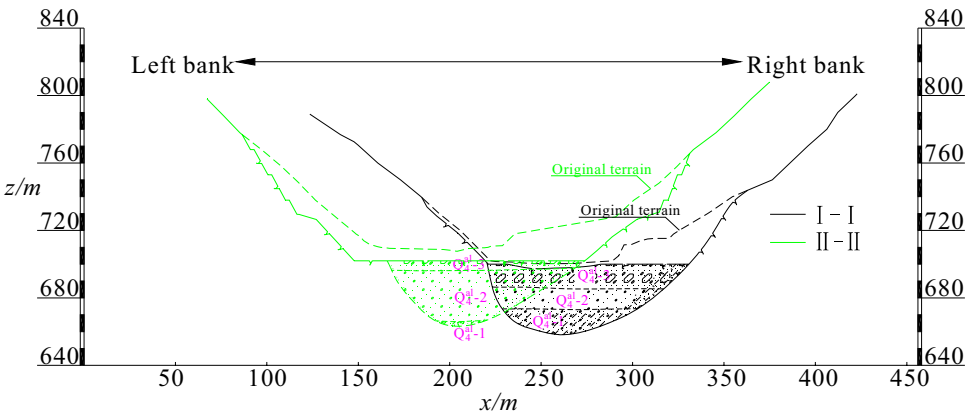

Fig. 5 Cross section of the valley terrain

Duncan–Chang E–B model [25], Lade model [13], and elastic–plastic model [26] are used to predict dam deformation during construction. The creep model [9] is used to simulate rockfill behavior during the dam operation period. The Duncan–Chang E–B model, proposed by Duncan et al., is the most widely used model for rockfill behavior in the construction [9, 27, 28]. The Duncan–Chang E–B model is used to describe rockfill behavior in the Miaojiaba CFRD. Triaxial tests are conducted to obtain the mechanical parameters of rockfill materials. The parameters of the Duncan–Chang E–B model are listed in Table 3.

The face slab and toe slab are modeled as linear elastic material with Young's modulus of 28 GPa and Poisson's ratio (ν) of 0.167, and the cutoff wall with Young's modulus of 26 GPa. The density of concrete material is 2450 kg/m^3. A strong contact interaction occurs among the face slab, cutoff wall, and adjacent gravel layer because of the significant difference in their stiffness. Thus, simulating the contact interaction among the face slab, cutoff wall, and adjacent gravel layer is important. The contact interaction is modeled using no-thickness friction contact method based on the ADINA [29] systems.

4.2 Typical Valley Terrain

The influence of valley terrain is considered [2] as a significant factor within the dam because of arching across the abutment slopes. Thus, investigating the influence of abutment slope variety on the deformation of CFRD is significant for understanding CFRD behavior and constructing CFRD under different valley terrains. Three types of typical valley terrain are investigated to compare the effect of valley terrain on the deformation behavior of CFRDs built on alluvium. As shown in Fig. 6, the terrain shape line is assumed to be constant at the downstream slope foot and the abutment slope angle increases linearly from upstream to downstream. In the first valley terrain, the abutment slope angle is constant from upstream to downstream. In the second valley terrain, the left abutment slope angle gradually increases from upstream to downstream. In the third valley terrain, both abutment slope angles of gradually increase from upstream to downstream.

4.3 Numerical Model

The 3D FE mesh models of three types of valley terrain are established in numerical analysis. The 3D FE mesh model of the second valley terrain is presented in Fig. 7. The embankment cross-section is divided into four main zones: cushion zone 2A, transition zone 3A, main rockfill zone 3B, and sub rockfill zone 3C. The model is discretized into 50,260 elements. Eight-node isoparametric elements are used for meshing. The alluvium is divided into three layers in accordance with geological properties. The face slab and cutoff wall are discretized into three layers along the thickness direction to accurately reflect their behavior.

The construction of the Miaojiaba CFRD started on October 30, 2009, and it was completed after 15 months. The entire section of the rockfill was constructed at an elevation of 740 m on March 31, 2010. Subsequently, the entire section of the rockfill was constructed at an elevation of 780 m from April 1, 2010 to October 15, 2010. The rockfill construction was completed on November 1, 2010. The impounding process of the reservoir was from March 9 to July 7, 2011. The construction and impounding comprise 33 steps based on the actual construction schedule. As shown in Fig. 8, the first 24 steps simulate the rockfill placement with 5 m lifts, and the 25th–28th steps simulate the face slab cast. The 29th–33rd steps simulate the initial impoundment of elevation from 700 m to 800 m with five height increments (Fig. 9). The loading path of the CFRD in the modeling process is consistent with the actual construction schedule. The water pressure at upstream is simulated as hydrostatic pressure on the face slab. The bottom boundary of the model is fixed in the x-, y-, and z-directions. The side boundary of the model is constrained in the normal direction.

5 Results and Discussion

5.1 Face Slab Deformation After Initial Impoundment

The distribution of the face slab deflection is shown in Fig. 10. No significant difference is observed with the

Table 3 Duncan–Chang E–B model parameters of the Miaojiaba CFRD

Material	Density (kg/m^3)	K	n	K_{ur}	φ_0 (°)	n_{ur}	c (kPa)	Rf	Kb	m
2A	2250	1400	0.42	2200	49	0.38	0	0.85	750	0.20
3A	2230	1300	0.42	2100	49	0.38	0	0.85	740	0.20
3B	2300	1250	0.45	1950	53	0.40	0	0.90	600	0.40
3C	2150	1050	0.35	1450	52	0.39	0	0.81	570	0.32
$Q_4^{al}-1$	2050	1000	0.43	1500	43	0.43	0	0.78	550	0.30
$Q_4^{al}-2$	2050	1200	0.43	1700	42	0.43	0	0.80	600	0.30
$Q_4^{al}-3$	2100	1500	0.42	2000	41	0.42	0	0.81	650	0.20

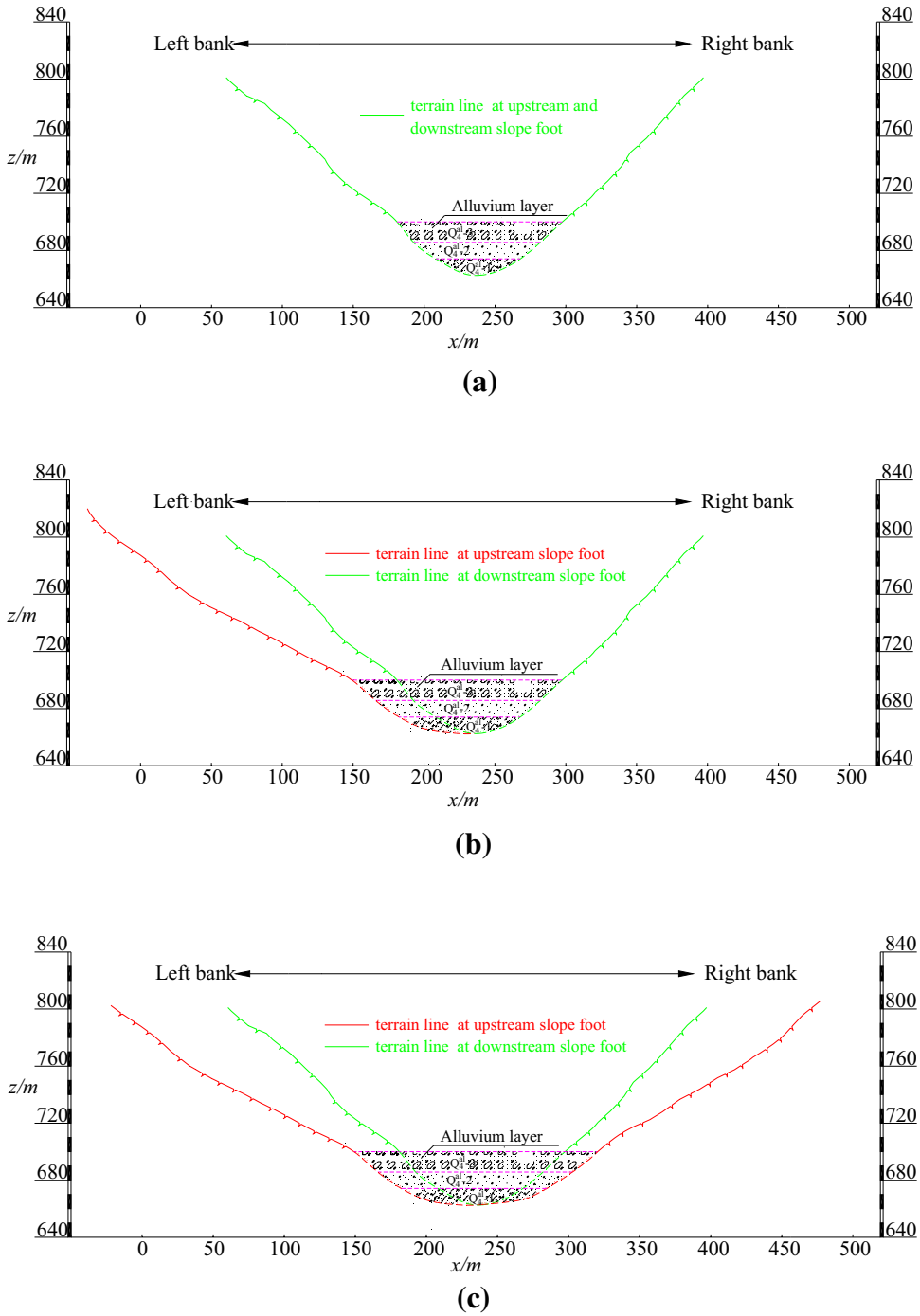

Fig. 6 Three types of typical valley terrain. **a** Constant abutment slope angle from upstream to downstream. **b** Gradual increase of the left abutment slope angle from upstream to downstream. **c** Gradual increase of the both abutment slope angles from upstream to downstream

maximum deflection of the face slab after initial impoundment. However, the distribution of the deflection presents a significant difference. Unlike the abutment slope angle, which is constant from upstream to downstream, the deflection contours of the left half of the face slab extends toward the left abutment. Moreover, the right half of the face slab deflection distribution shows no significant difference when the slope angle of the left abutment gradually increases from upstream to downstream. This feature may indicate that torsional deformation exists in the face slab, and the influence sphere is located only in half of the face slab. In addition, the position of maximum deflection shifts toward the left abutment, and the deflection gradient of the right half is larger than that of the left half of the face slab mainly because of torsional deformation in the CFRD. The deflection distribution is generally symmetric, whereas the deflection contours extends toward both abutments when the double abutment slope angles

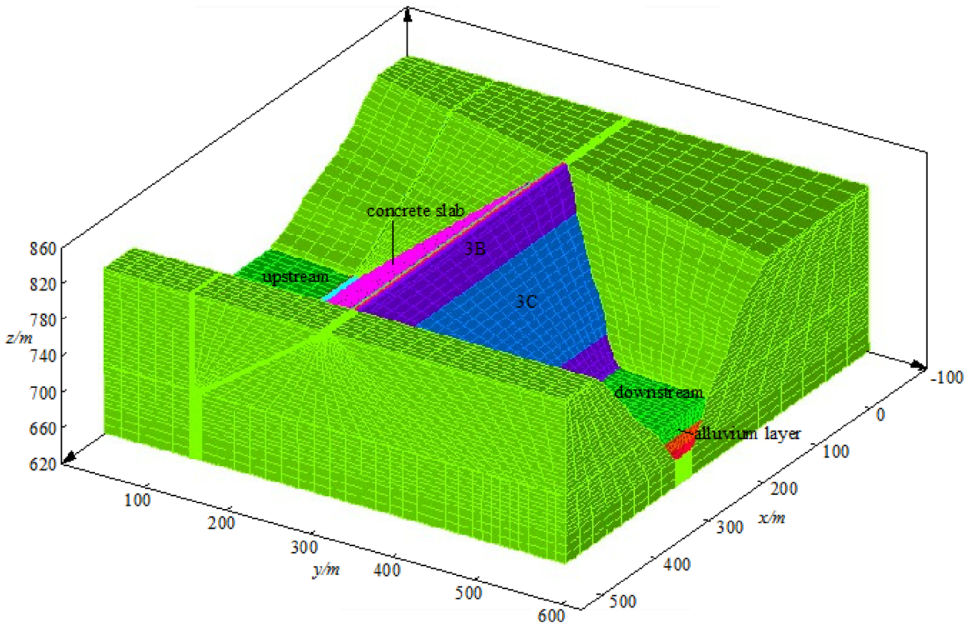

Fig. 7 3D FE mesh model of the second valley terrain

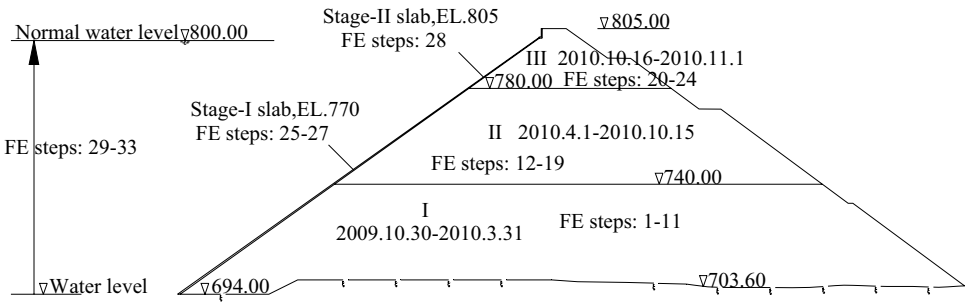

Fig. 8 Construction schedule of the Miaojiaba CFRD

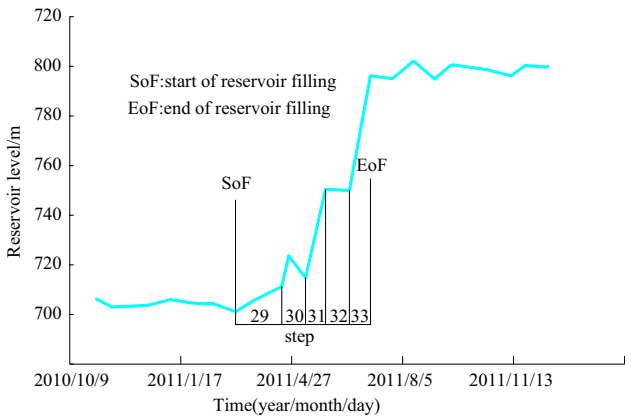

Fig. 9 Impoundment schedule of Miaojiaba CFRD

gradually increase from upstream to downstream. This phenomenon is caused by the increase of the valley shape factor A/H^2 (A, upstream slope face area; H: dam height) due to the abutment slope angle variety from upstream to downstream.

The face slab displacement along the dam axis is shown in Fig. 11. When the abutment slope angle is constant from upstream to downstream, the face slab displacement along the dam axis is symmetric because the valley terrain is approximately symmetric. However, the face slab displacement along the dam axis is asymmetric with the left abutment slope angle increasing from upstream to downstream. The valley asymmetry results indicate that the rockfill displacement along the dam axis near the left abutment is smaller than that near the right abutment, which directly affects the behavior of the face slab. The influence sphere is approximately located in half of the face slab, and the influence boundary presents an "S" shape in Fig. 11a. The influence on the right half of the face slab is negligible, and the influence width varies nonlinearly. As shown in Fig. 11b, the maximum influence width is located in the upper portion of the face slab. This result is caused mainly by arching across the abutment slopes. The arching effect is noticeable at the lower portion of the dam, and this effect is weakened gradually and disappears at the upper portion of face slab with abutment slope variety.

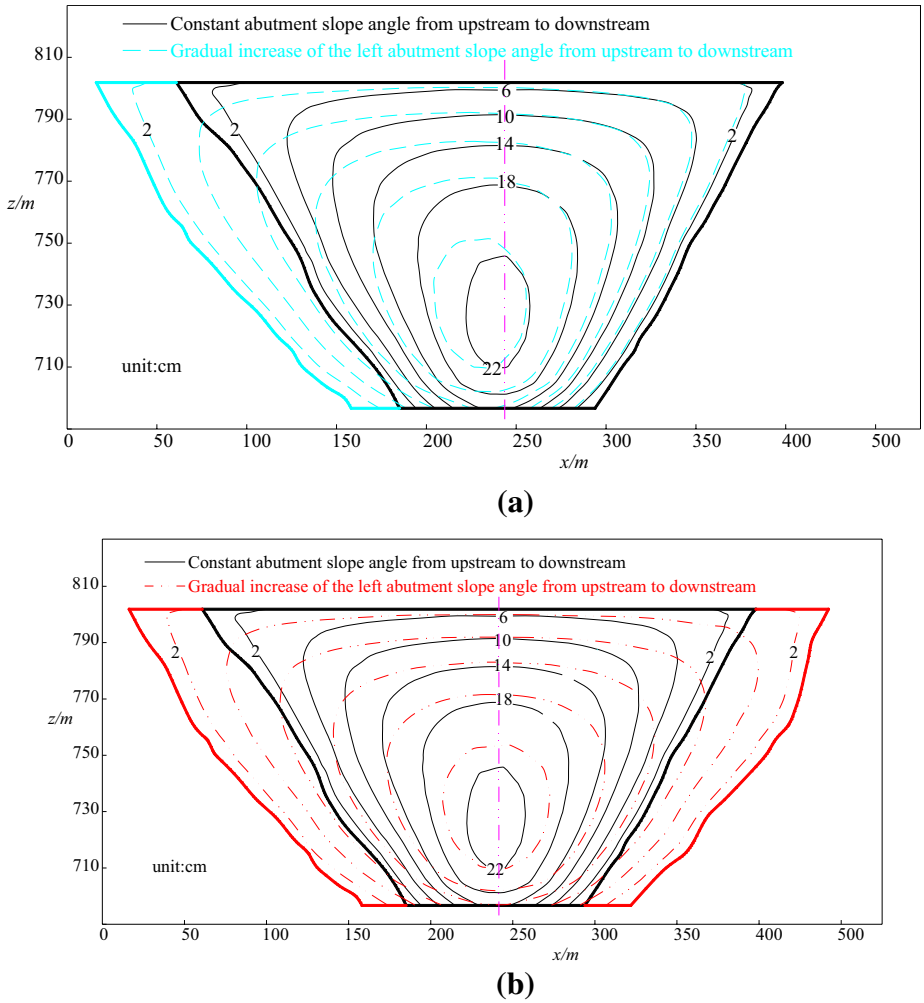

Fig. 10 Distribution of the face slab deflection. **a** Gradual increase of the left abutment slope angle from upstream to downstream. **b** Gradual increase of the both abutment slope angles from upstream to downstream

5.2 Dam Deformation After Initial Impoundment

The internal settlement in cross section 0 + 192 is compared, as shown in Fig. 12. Generally, the settlement results are similar. The maximum settlements are observed at the lower portion of the dam with the influence of alluvium compression deformation, which differs from the dam settlements built on the bedrock. In comparison with the abutment slope angle, which is constant from upstream to downstream, the maximum settlement increases with the abutment slope angle increasing from upstream to downstream. Particularly, when both abutment slope angles increase from upstream to downstream, the maximum settlement increases by 10.3%.

The distribution of the dam crest settlements of the three types of typical valley terrain is shown in Fig. 13. The maximum dam crest settlement is observed at the center of the dam crest. When the left abutment slope angle increases from upstream to downstream, the dam crest settlement near the left abutment increases, whereas that near the right abutment slightly varies. In addition, the position of the maximum dam crest settlement shifts toward the left abutment. These results indicate that the variety of both abutment slope angles from upstream to downstream has a noticeable effect on the dam crest settlement near the abutment slope, whereas the maximum dam crest settlement only slightly varies.

5.3 Major Principal Stress After Initial Impoundment

The major principal stress contours in cross section III–III of the three types of typical valley terrain are presented in Fig. 14. The abutment slope angle variation has a minimal effect on the distribution of the principal stresses in the longitudinal cross section. The major principal stress at the lower portion of the dam increases slightly with the abutment slope angle increasing from upstream to downstream, whereas the major principal stress variation at the upper portion of the dam is negligible. The reasons behind the results can be summarized as follows. In comparison with the abutment slope angle, which is constant from upstream to downstream, the volume of the rockfill increases with the

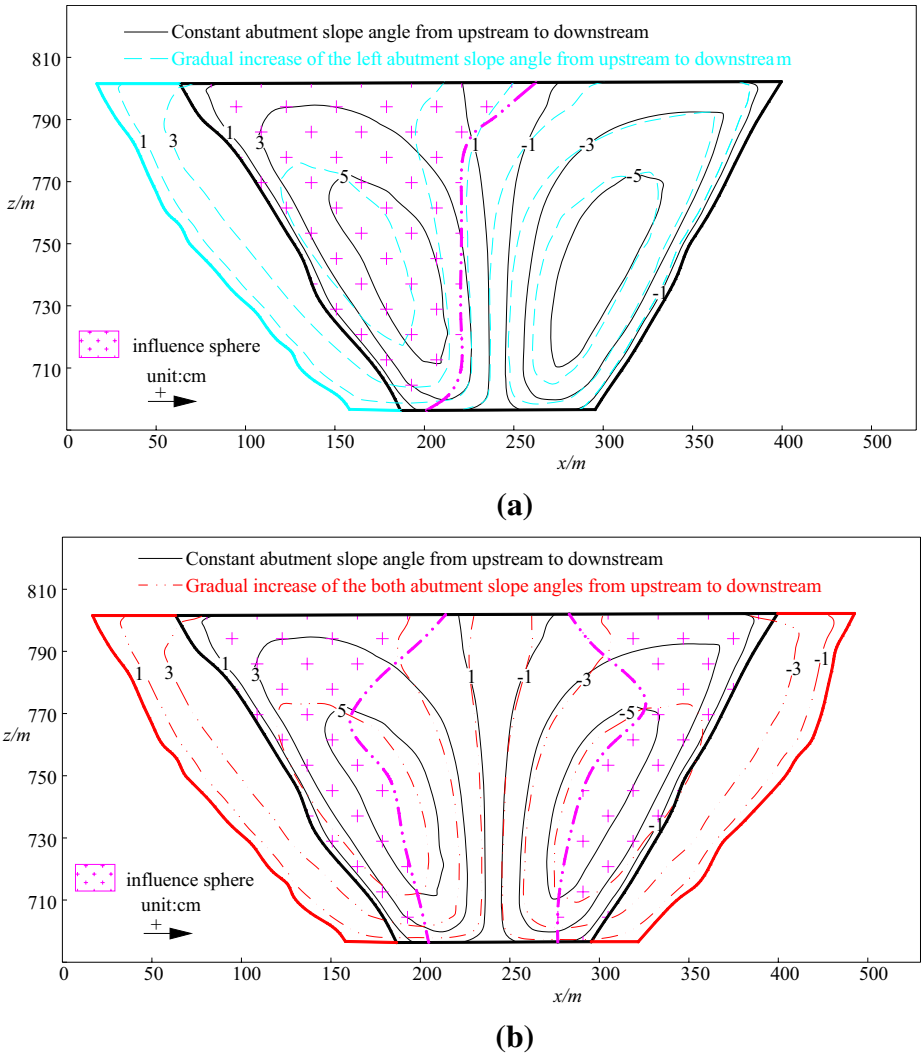

Fig. 11 Face slab displacement along the dam axis. **a** Gradual increase of the left abutment slope angle from upstream to downstream. **b** Gradual increase of the both abutment slope angles from upstream to downstream

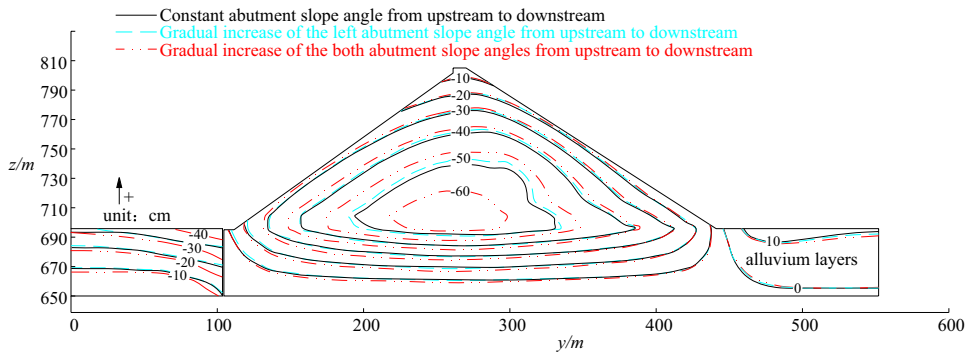

Fig. 12 Internal settlements in cross section 0 + 192

abutment slope angle increasing from upstream to downstream, thereby increasing the deformation and stress of the rockfill. Moreover, the terrain shape line is assumed to be constant at the downstream slope foot. The increase of the abutment slope angle from upstream to downstream weakens the restraint of the bedrock to the dam, thereby mitigating the arching effect and leading to major principal stress increase at the lower portion of the dam. The left abutment slope angle increases from upstream to downstream, which causes greater major principal stress on the left abutment than on the right abutment at the same elevation and results in a torsion effect in the dam stress distribution.

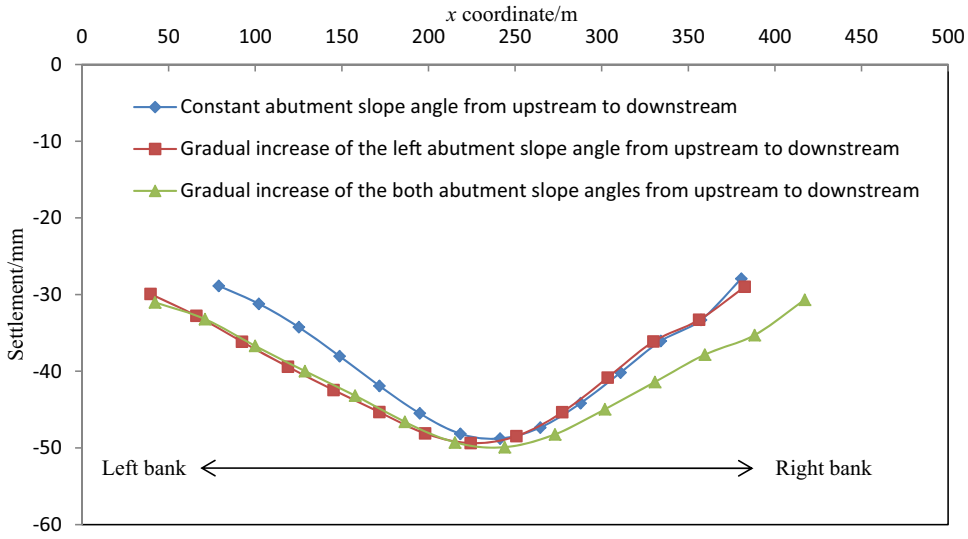

Fig. 13 Distribution of dam crest settlements

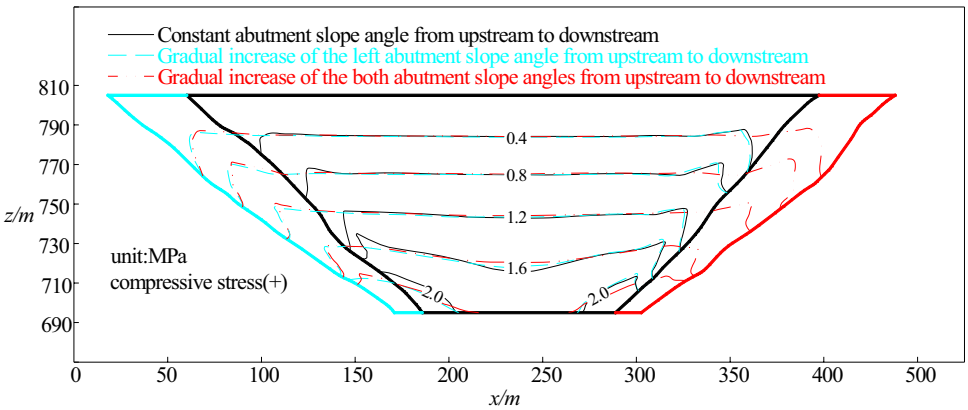

Fig. 14 Major principal stress contours in cross section III–III

6 Case Study

The Zipingpu CFRD is presented as a case study to illustrate the generality of the results in this study. The Zipingpu CFRD was built on Minjiang River in northwestern Chengdu, Sichuan Province, China. The dam is designed with a maximum height of 156 m and crest length of 634.8 m. It has a storage capacity of 1.112 billion m^3. The powerhouse has an installed capacity of 760 MW. The upstream slope is 1v:1.4 h, and the downstream local slopes are 1v:1.5 h and 1v:1.4 h.

The valley terrain and layout view of the Zipingpu CFRD is shown in Fig. 15. The dam lies on the end of a U-shaped river bend, which has been incised by the Minjiang River. The dam rests mostly on recent alluvium consisting of erratic boulders and gravel. The alluvium in a zone of approximately 100 m width downstream from the plinth is excavated and the remaining alluvium attains a maximum thickness of 14 m beneath the dam. The river valley cross section is an unsymmetrical V shape. The right abutment slope varies significantly from upstream to downstream. The right abutment slope is approximately 18° at the upstream slope foot, and which is approximately 30° at the downstream slope foot.

The Zipingpu CFRD was analyzed by Xu and Zou [6] based on a generalized plasticity model. The face slab deflection after initial impoundment is shown in Fig. 16. The deflection gradient of the left half of the face slab is larger than that of the right half of the face slab. The maximum deflection slightly shifts toward the right abutment. The maximum deflection is observed at the higher third of the face slab mainly because the maximum thickness of alluvium is only 14 m compared with dam height. The face slab displacement along the dam axis [30] is presented in Fig. 17. The displacement along the dam axis at the right abutment is smaller than that at the left abutment, with the right abutment slope increasing from upstream to downstream. The maximum displacement is observed at the left abutment slope. These features are consistent with the results in this study. Hence, results in this work can

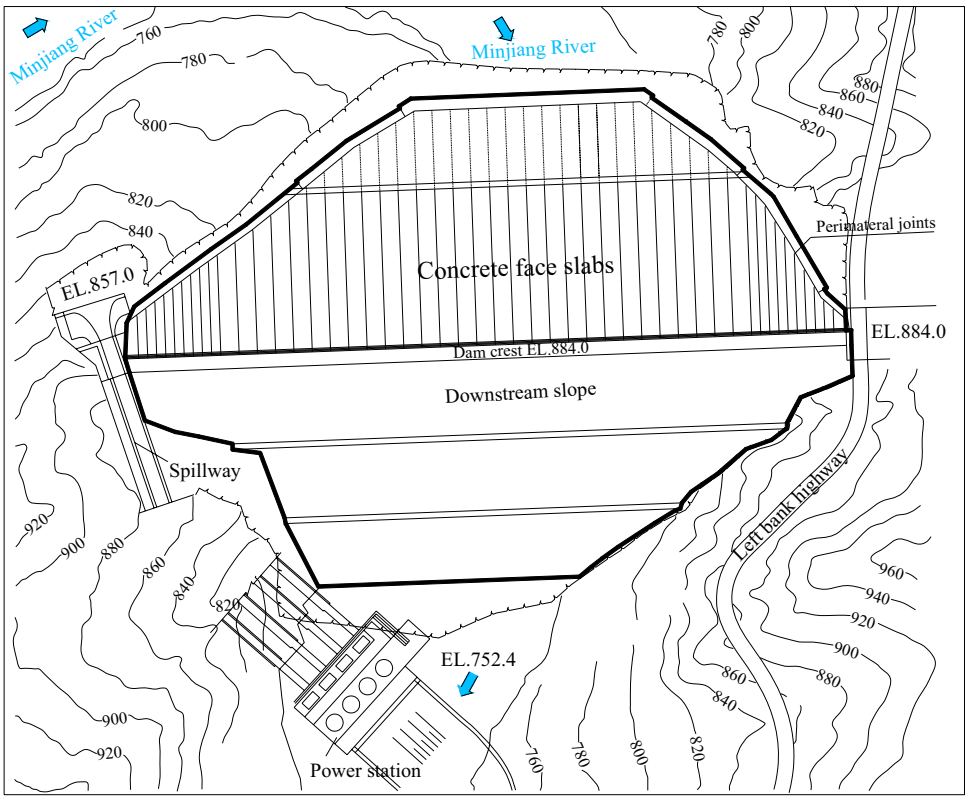

Fig. 15 Valley terrain and layout of the Zipingpu CFRD

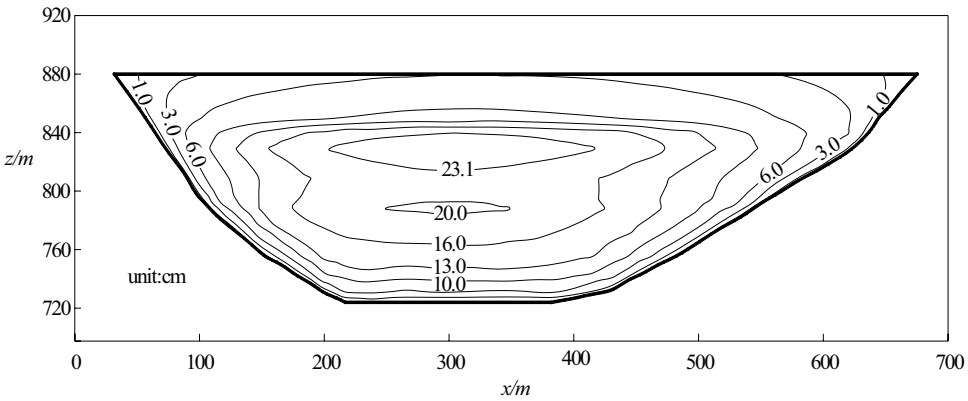

Fig. 16 Distribution of the Zipingpu face slab deflection

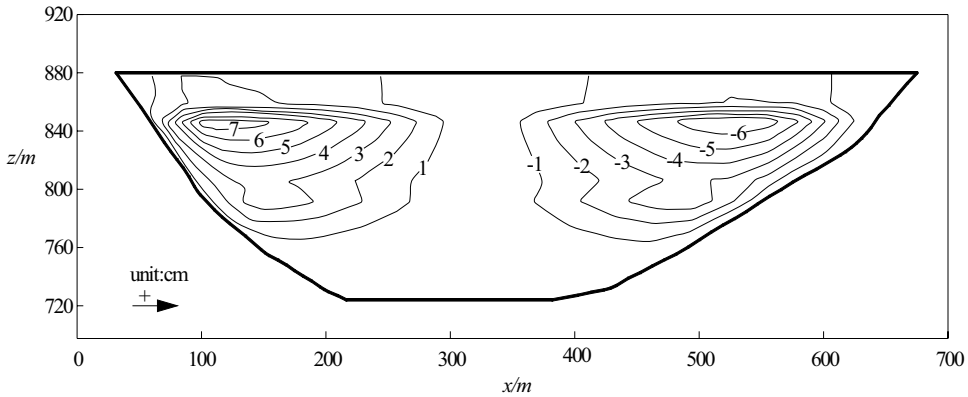

Fig. 17 Zipingpu face slab displacement along the dam axis

provide a general understanding of the effect of abutment slope angle on the behavior of CFRDs built on alluvium.

7 Conclusions

In this study, the influence of the variety of abutment slope angles on the deformation and stress of CFRDs is investigated. The Zipingpu CFRD is presented as a case study to illustrate the generality of the results in this work. The following conclusions can be drawn from the results:

1. The parameter joint deformation will slightly increase with the abutment slope angle under the condition that it is less than 55°. Oversteepened abutment slope significantly increases the magnitude of perimeter joint deformation. A special compaction zone at the oversteepened abutment slope must be designed to minimize perimeter joint deformation.
2. The variety of abutment slope angles from upstream to downstream causes distribution differences of the face slab deflection and displacement along the dam axis. The influence sphere is approximately located at half of the face slab with a single abutment slope angle variety from upstream to downstream. The effect on the face slab displacement along the dam axis is more significant at the upper portion than that at the lower portion of the face slab. The valley asymmetry causes the deformation gradient of the face slab at the steep abutment slope to be larger than that at the flat abutment slope. Reducing of concrete slab width at the steep abutment slope can effectively mitigation the potential of cracks on the concrete slab.
3. The variety of abutment slope angles from upstream to downstream may weaken the arching across abutment slopes and remarkably affect the dam crest settlement near the abutment, however, it has a negligible effect on the maximum dam crest settlement. The varying single abutment slope angle from upstream to downstream causes valley asymmetry, and the position of the maximum crest settlement shifts toward the flatter abutment slope.
4. The increase of abutment slope angles from upstream to downstream increases the principal stress at the lower-fourth portion of the rockfill. A varying single abutment slope from upstream to downstream may cause torsion effect on dam stress distribution.

Acknowledgements The authors acknowledge the support provided by the National Natural Science Foundation of China (51679197, 51679193, and 51409208), Natural Science Basic Research Program of Shanxi Province - Key Project (2017JZ013) and the State Key Laboratory of Geo-information Engineering (SKLGIE2017-M-4-4). The authors would like to thank the editor and anonymous reviewers for their constructive criticism of the manuscript. Their efforts improve the quality of the paper.

References

1. Chen Y, Hu R, Lu W, Li D, Zhou C (2011) Modeling coupled processes of non-steady seepage flow and non-linear deformation for a concrete-faced rockfill dam. Comput Struct 89(13):1333–1351
2. Hunter G, Fell R (2003) Rockfill modulus and settlement of concrete face rockfill dams. J Geotech Geoenviron Eng 129(10):909–917
3. Dakoulas P (2012) Nonlinear seismic response of tall concrete-faced rockfill dams in narrow canyons. Soil Dynamics Earthquake Engineering 34(1):11–24
4. Dakoulas P (2012) Longitudinal vibrations of tall concrete faced rockfill dams in narrow canyons. Soil Dyn Earthq Eng 41:44–58
5. Kim M-K, Lee S-H, Choo YW, Kim D-S (2011) Seismic behaviors of earth-core and concrete-faced rock-fill dams by dynamic centrifuge tests. Soil Dyn Earthq Eng 31(11):1579–1593
6. Xu B, Zou D, Liu H (2012) Three-dimensional simulation of the construction process of the Zipingpu concrete face rockfill dam based on a generalized plasticity model. Comput Geotech 43:143–154
7. Modares M, Quiroz JE (2015) Structural analysis framework for concrete-faced Rockfill Dams. Int J Geomech 16(1):04015024
8. Kim Y-S, Kim B-T (2008) Prediction of relative crest settlement of concrete-faced rockfill dams analyzed using an artificial neural network model. Comput Geotech 35(3):313–322
9. Zhou W, Hua J, Chang X, Zhou C (2011) Settlement analysis of the Shuibuya concrete-face rockfill dam. Comput Geotech 38(2):269–280
10. Haghbin M (2016) Bearing capacity of strip footings resting on granular soil overlying soft clay. Int J Civil Eng 14(7):467–477
11. Dob H, Messast S, Mendjel A, Boulon M, Flavigny E (2016) Behavior of sand after a high number of cycles application to shallow foundation. Int J Civil Eng 14(7):459–465
12. Bayat M, Ghalandarzadeh A (2017) Stiffness degradation and damping ratio of sand-gravel mixtures under Saturated State. Int J Civil Eng 1–17
13. Lollino P, Cotecchia F, Zdravkovic L, Potts DM (2005) Numerical analysis and monitoring of Pappadai dam. Can Geotech J 42(6):1631–1643
14. Karim MR, Gnanendran CT, Lo SCR, Mak J (2010) Predicting the long-term performance of a wide embankment on soft soil using an elastic–viscoplastic model. Can Geotech J 47(2):244–257
15. Ozcoban S, Berilgen MM, Kilic H, Edil TB, Kutay Ozaydin I (2007) Staged construction and settlement of a dam founded on soft clay. J Geotech Geoenviron Eng 133(8):1003–1016
16. Oliveira PJV, Lemos LJ, Coelho PA (2009) Behavior of an atypical embankment on soft soil: field observations and numerical simulation. J Geotech Geoenviron Eng 136(1):35–47
17. Lo SR, Mak J, Gnanendran CT, Zhang R, Manivannan G (2008) Long-term performance of a wide embankment on soft clay improved with prefabricated vertical drains. Can Geotech J 45(8):1073–1091
18. den Haan E, Feddema A (2013) Deformation and strength of embankments on soft Dutch soil. In: Proceedings of the Institution of Civil Engineers-Geotechnical Engineering 166(3):239–252
19. Kovacevic N, Higgins K, Potts D, Vaughan P (eds) (2011) Undrained behaviour of brecciated upper lias clay at Empingham dam. Stiff Sedimentary Clays: Genesis and Engineering Behaviour: Géotechnique Symposium in Print 2007; Thomas Telford Ltd

20. Yin Z-Y, Karstunen M, Chang CS, Koskinen M, Lojander M (2011) Modeling time-dependent behavior of soft sensitive clay. J Geotech Geoenviron Eng 137(11):1103–1113
21. Cooke JB (1984) Progress in rockfill dams. J Geotech Eng 110(10):1381–1414
22. Cooke JB, Sherard JL (eds) (1985) Concrete Face Rockfill Dams—Design. ASCE, Reston
23. Filho F, de SPinto N (2005) CFRD dam characteristics learned from experience. Int J Hydropower Dams 12(1):72
24. Amaya F, Marulanda A (eds) (1985) Golillas Dam—Design. ASCE, Reston
25. Clough GW, Duncan JM (1971) Finite element analyses of retaining wall behavior. J Soil Mech Found Div 97(12):1657–1673
26. Zhang G, Zhang J-M (2009) Numerical modeling of soil–structure interface of a concrete-faced rockfill dam. Comput Geotech 36(5):762–772
27. Xing H-F, Gong X-N, Zhou X-G, Fu H-F (2006) Construction of concrete-faced rockfill dams with weak rocks. J Geotech Geoenviron Eng 132(6):778–785
28. Saboya F, Byrne P (1993) Parameters for stress and deformation analysis of rockfill dams. Can Geotech J 30(4):690–701
29. Bathe K (2002) Theory and modeling guide. ADINA R & D, Watertown
30. Gang L, Jian-min Z, Zhu-jiang S (2002) 3-D stress-displacement analysis for Zipingpu concrete faced rockfill dam. J Hydroelectr Eng 1:13–18